

Bright transients from strongly-magnetized neutron star-black hole mergers

Daniel J. D’Orazio*

Department of Astronomy, Columbia University, New York, New York 10027, USA

Janna Levin

*Department of Physics and Astronomy, Barnard College,
Columbia University, New York, New York 10027, USA*

Norman W. Murray†

*Canadian Institute for Theoretical Astrophysics, 60 Street George Street,
University of Toronto, Toronto, Ontario M5S 3H8, Canada*

Larry Price

Division of Physics, Mathematics, and Astronomy, California Institute of Technology, Pasadena, California 91125, USA

Direct detection of black hole-neutron star pairs is anticipated with the advent of aLIGO. Electromagnetic counterparts may be crucial for a confident gravitational-wave detection as well as for extraction of astronomical information. Yet black hole-neutron star pairs are notoriously dark and so inaccessible to telescopes. Contrary to this expectation, a bright electromagnetic transient can occur in the final moments before merger as long as the neutron star is highly magnetized. The orbital motion of the neutron star magnet creates a Faraday flux and corresponding power available for luminosity. A spectrum of curvature radiation ramps up until the rapid injection of energy ignites a fireball, which would appear as an energetic blackbody peaking in the x ray to γ rays for neutron star field strengths ranging from 10^{12} G to 10^{16} G respectively and a $10M_{\odot}$ black hole. The fireball event may last from a few milliseconds to a few seconds depending on the neutron star magnetic-field strength, and may be observable with the Fermi Gamma-Ray Burst Monitor with a rate up to a few per year for neutron star field strengths $\gtrsim 10^{14}$ G. We also discuss a possible decaying post-merger event which could accompany this signal. As an electromagnetic counterpart to these otherwise dark pairs, the black-hole battery should be of great value to the development of multi-messenger astronomy in the era of aLIGO.

I. INTRODUCTION

Black holes are dark dead stars. Neutron stars are giant magnets. As the neutron star (NS) whips around the black hole (BH) in the final stages in the life of a pair, an electromotive force (emf) is generated that is powerful enough to light a beacon, which conceivably we might observe at cosmological distances [1, 2]. The battery could power synchrocurvature radiation, a blazing fireball, or relativistic jets.

Famously, tidal disruption of a NS is expected to generate a gamma-ray burst after merger [3]. However, it is underappreciated that most BHs should be large enough ($\gtrsim 6M_{\odot}$) to swallow their NSs whole and so no gamma-ray burst is expected from typical pairs [4]. Therefore, our BH battery, which operates with the NS intact, may be one of the only significant sources of electromagnetic luminosity for coalescing BHNS binaries.¹ An observation of such a transient would be exciting in its own right. Advanced gravitational-wave detectors [*e.g.*, 7], with the prospect of multi-messenger astronomy, provide added incentive for the more detailed predictions of the electromagnetic (EM) signatures we present here.

Even with the benefit of nearly fifty years of observa-

tions, common NS pulsars require theoretical attention. If the decades of pulsar research offer a sociological lesson, it would be that the details of the electromagnetic processes are not easy to model, that the mechanisms at work are not obvious. Without the benefit of observations, we would not presume to offer a definitive or complete electromagnetic portrait of the BHNS engine. But we can sketch plausible emission mechanisms to encourage first searches for these potentially important transients.

As already argued in the original references [1, 2], curvature radiation is a natural channel for luminosity. We examine the spectrum of curvature radiation here. (We mention that another intriguing channel for some fraction of the battery power could be radio emission through coherent processes, providing the correct time scales and energetics for a subclass of the fast radio bursts [8].) We conclude that, just before merger, when the power is greatest, curvature radiation results in copious pair production which fuels a fireball. The fireball expands under its own pressure until the photosphere radiates as a blackbody peaking in the hard x-ray to γ -ray range for milliseconds (msec) to seconds depending on NS magnetic-field strength.

If the merger were to happen in our own galaxy, we might watch the spectrum of curvature radiation ramp up followed by the brighter fireball. At cosmological distances, the high-energy lead up in curvature radiation will be too faint to detect, but the fireball could be observable at a rate of at least a few per year with the FERMI Gamma-Ray Burst Monitor (GBM), for NSs with $\gtrsim 10^{14}$ G surface magnetic fields. Such events

*Electronic address: dorazio@astro.columbia.edu

†Canada Research Chair in Astrophysics

¹ Resonant shattering of the NS crust could also generate an interesting electromagnetic signature for nondisrupting systems [5, 6].

could possibly be a subclass of short gamma-ray bursts. Since the fireball takes at least $\sim 0.2\text{ms}$ to 0.02s to expand and release the light, the burst from the fireball would lag just behind the peak gravitational-wave emission. Post-merger, the transfer of magnetic flux on to the black hole might lead to a brief jet and afterglow. Pre- and post-merger triggered events could be observed to occur very close to each other in timing. We hope the predicted transient discussed here encourages observational interest.

A. The power of the battery

First, we review the estimate of the energy budget for the BH battery. The BHNS system behaves analogously to a unipolar inductor, which has been investigated in application to a number of other astrophysical systems, *e.g.* Jupiter and its moon Io [9], planets around white dwarfs [10] and main sequence stars [11, 12], binary neutron stars [13–16], compact white dwarf binaries [15, 17–19], BHs boosted through magnetic fields [20, 21], and the Blandford-Znajek (BZ) mechanism [22] for a single BH spinning in a magnetic field [for recent numerical work on the BZ mechanism see *e.g.* 23, 24]. The calculation for BHNS systems, already presented in Ref. [1] and confirmed in the detailed relativistic analysis of Ref. [2], as well as the numerical calculations of Ref. [25], gives the scaling of power available for conversion into electromagnetic luminosity. In the next section we will consider the implications of throwing this power into luminous elements in the BHNS circuit.

For observers which have not fallen through, the BH horizon is well approximated, electromagnetically, as a conducting sphere [26]. The relative motion of the BH through the magnetic field of the NS induces an emf. We visualize the circuit which generates this emf in Figure 1. Because charged particles are bound to a given field line, we imagine that one set of field lines forms one set of wires in a closed circuit. In conceptualizing the circuit it is important to distinguish between field lines that act as wires at a given instant and those that contribute to the changing magnetic flux through the circuit. The circuit is closed by connecting the wires along the surface of the horizon, as in the snapshot of Figure 1. As the BHNS pair orbits, the circuit sweeps through the dipole field. The changing magnetic flux through a surface bounded by the changing circuit corresponds to an emf. There are an infinite number of such circuits as different field lines intersect the BH.

Following Ref. [1], the voltage generated is given by

$$\begin{aligned} V_{\mathcal{H}} &= \int \alpha \mathbf{E} \cdot d\mathbf{s} = -\frac{1}{c} \frac{d}{dt} \int \alpha \mathbf{B} \cdot d\mathbf{A} \\ &= -\oint \alpha \left(\frac{\mathbf{v}}{c} \times \mathbf{B} \right) \cdot d\mathbf{s}, \end{aligned} \quad (1)$$

where \mathbf{v} is the relative velocity of the BH horizon with respect to magnetic-field lines and we add a factor of the lapse function for a spinning BH α by hand to account for the gravita-

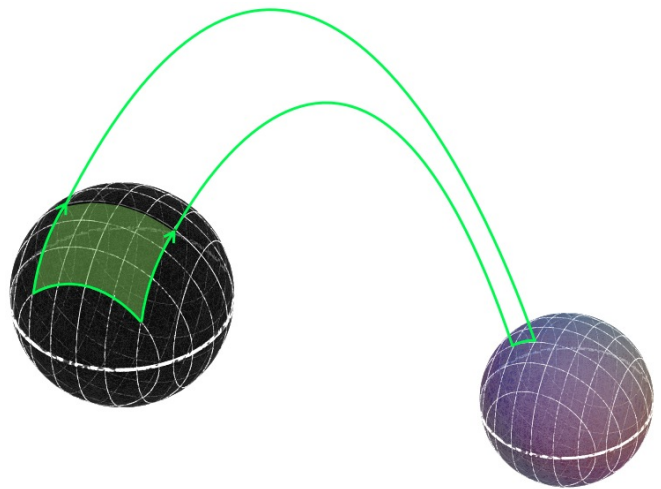


FIG. 1: Schematic of a Faraday loop as seen by an observer external to the horizon. The black sphere depicts the BH horizon orbiting out of the page. In green is a schematic of the instantaneous closed loop defining one of infinitely many circuits made up of electrons and positrons moving along magnetic-field lines which trace the BH horizon.

tional redshifts.² Given a dipole magnetic field, which drops off with distance from the NS as r^{-3} , anchored on the NS with radius R_{NS} (taken to be 10 km throughout) and surface magnetic-field strength B_{NS} ,

$$B(r) = B_{\text{NS}} \left(\frac{R_{\text{NS}}}{r} \right)^3, \quad (3)$$

the voltage (1) acquires a contribution only from the integral along the horizon in the direction of the line connecting the BH and NS, and so evaluates to

$$V_{\mathcal{H}} = 2R_H \left[\frac{r(\Omega_{\text{orb}} - \Omega_{\text{NS}})}{c} + \frac{S}{4\sqrt{2}} \right] B_{\text{NS}} \left(\frac{R_{\text{NS}}}{r} \right)^3, \quad (4)$$

where R_H is the radius of the horizon and where we have included a factor to account for the spin, $0 \leq S \leq 1$, of the BH [1]. Notice that in Eq. (3), B_{NS} drops off with distance from the NS, so the voltage varies across the horizon for small binary separations. In the limit in which we ignore the finite size of the compact objects, we interpret r as the binary separation.

² In Boyer-Lindquist coordinates for a Kerr BH,

$$\begin{aligned} \alpha &= \frac{\rho}{\Sigma} \sqrt{\Delta} \\ \rho &= (\mathcal{z}^2 + S^2 \cos^2 \theta)^{1/2} \\ \Sigma &= ([\mathcal{z}^2 + S^2] - S^2 \Delta \sin^2 \theta)^{1/2}. \end{aligned} \quad (2)$$

for BH spin $S \leq 1$. Here we use \mathcal{z} for the distance from the BH to be distinguished from the distance from the neutron star r .

The total power that can be liberated by the battery is

$$\mathcal{P}(t) = \frac{V_{\mathcal{H}}^2(t)}{(\mathcal{R}_{\mathcal{H}} + \mathcal{R}_{\text{NS}})^2} \mathcal{R}_{\text{NS}}. \quad (5)$$

The resistance across the horizon of the BH is $\mathcal{R}_{\mathcal{H}} = 4\pi/c \text{ cm}^{-1}\text{s}$. Since the effective resistance of the NS and its magnetosphere (\mathcal{R}_{NS}) is unknown, we choose $\mathcal{R}_{\text{NS}} = \mathcal{R}_{\mathcal{H}}$ to give the largest possible luminosities. This impedance matching condition is the same as that imposed to derive the Blandford-Znajek power [22], in which case the angular velocity of magnetic-field lines at infinity are set to one half of the BH horizon angular velocity [26, 27].

The power scales roughly as

$$\mathcal{P} \sim M^2 B_{\text{NS}}^2 r^{-6} v^2. \quad (6)$$

At large separations $v^2 \sim M/r$ is small, climbing to near the speed of light at merger. Measuring length in units of M , the power scales as

$$\mathcal{P} \sim B_{\text{NS}}^2 M^{-4} v^2. \quad (7)$$

For a fixed number of gravitational radii between the NS surface and the BH horizon, a larger BH boosts the power as M^2 , but the larger implied distance between the two decreases the magnetic-field strength at the horizon by M^{-6} .

We discuss briefly when these scalings break down. In the limit that the NS and BH are close, and their finite sizes are important, the NS surface can come arbitrarily close to the BH horizon in which case $B_{\text{NS}}^2 r^{-6} \rightarrow B_{\text{NS}}^2$. Placing the NS surface at the horizon and spinning it with velocity v would generate power which increases with BH mass as $\mathcal{P} \sim M^2 B_{\text{NS}}^2 v^2$. If however, the BH mass was very large, the variation of the magnetic field across the BH horizon would become important. For very large BHs, the NS light cylinder will not span the horizon.³ In these cases, our assumption that the voltage drop is across the entire horizon breaks down and the power will scale more weakly than M^2 . In the present work, we ignore finite-size effects and take Eqs. (3)-(5) to be a good estimate of the average power available via the BH battery.

Here and throughout the rest of the paper we treat the NS surface magnetic-field strength as an unknown parameter. Because there are no observations of BHNS binaries, and hence no measurements of NS field strengths near merger with a BH, we have chosen a range in accordance with the observed NS fields [see *e.g.* 28]. We consider fields ranging from those of the radio pulsar population 10^{12} G up to the observed magnetar field strengths of a few times 10^{15} G [29] and beyond to larger, but not impossible field strengths of 10^{16} G,⁴ in order to

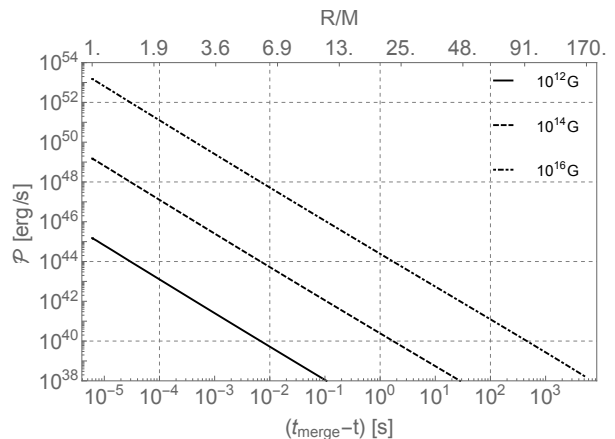


FIG. 2: Total possible power supplied by the BH battery via Eq. (5) as a function of time until merger for two point masses undergoing orbital decay via gravitational radiation reaction (Eq. 8). The solid, dashed, and dot-dashed lines indicate NS surface magnetic-field strengths of 10^{12} , 10^{14} , and 10^{16} G respectively, for a BH mass of $10M_{\odot}$. The plot extends to a binary separation of GM/c^2 , the size scale of the event horizon for the maximally spinning BH we consider. We have dropped factors of G and c in the axis labels.

probe the full range of energies available to the BHNS system. Conversely and as we discuss in §V, our models can constrain the NS field strength at merger.

In Figure 2, we plot the total power available for liberation by the binary as a function of time for varying NS magnetic field strengths and a maximally spinning BH of mass $10M_{\odot}$.⁵ Importantly, over the range of possible magnetic-field strengths, the energy liberated through the BH-battery mechanism is many orders of magnitude lower than that liberated by gravitational radiation [1], hence the orbital inspiral time scales are set by gravitational radiation loss and are robust despite different possible channels for the electromagnetic power. The time-dependent separation $r(t)$ decays due to gravitational radiation losses [31],

$$r(t) = \left(r^4(0) - 4 \frac{64}{5} \frac{G^3}{c^5} M_{\text{NS}} M (M + M_{\text{NS}}) t \right)^{1/4}, \quad (8)$$

where M_{NS} is the NS mass taken to be $1.4M_{\odot}$ throughout. Over the final second, the power available climbs by ~ 8 orders of magnitude. For a 10^{12} G dipole field, the power rises from pulsar scales $\sim 10^{36} \text{ erg s}^{-1}$ in that second, to $\sim 10^{44} \text{ erg s}^{-1}$ in the final millisecond (at $r = 2GM/c^2$). The power scales as B^2 reaching $10^{52} \text{ erg s}^{-1}$ for a magnetar with $B \sim 10^{16}$ G. For a maximally spinning BH, the horizon is at $r = GM/c^2$, so we extend the luminosity scaling

³ When the BH event horizon is larger than the size of the NS light cylinder, $M \gtrsim c^3 G^{-1} \Omega_{\text{NS}}^{-1} \sim 10^4 M_{\odot} 2\pi / \Omega_{\text{NS}}$, the full voltage drop of Eq. (4) cannot be realized.

⁴ NS field strengths as high as $\sim 10^{18}$ G are theoretically possible but would generate EM power that would rival the emission due to gravitational radiation and hence require numerical analysis.

⁵ Depending on the NS equation of state, the choice of a maximally spinning BH could cause the NS to be partially disrupted [*e.g.* 30]. In the same study, a BH spin $S \lesssim 0.95$ does not disrupt, and changing the spin by such a small amount has no notable impact on our results.

in Figure 2 down to this separation (noting that we still have $GM/c^2 > R_{\text{NS}}$ for $M \geq 7M_{\odot}$) where the luminosity peaks at $\sim 10^{45} \text{ erg s}^{-1} (B/10^{12} \text{ G})^2$.

Equation (5) gives an estimate of the power the battery could generate. Whether or not this power is available to light up the pair is the question at hand. We describe the most straightforward vehicles to convert the power into luminosity in the following sections.

II. CURVATURE RADIATION

The voltage drop will accelerate charges across magnetic-field lines connecting the NS to the BH. Basic physics suggests that these accelerated charges will provide a sensible channel for luminosity. The charges spiral around and are pushed along the magnetic fields when there is a parallel component of electric field, $\mathbf{E} \cdot \mathbf{B} \neq 0$. The result is a primary spectrum of curvature radiation.⁶

The extent to which the BH battery can act as a particle accelerator is mitigated by the conducting properties of the surrounding magnetosphere. The NS sustains a magnetosphere by pulling charges from the NS and through various pair production channels in the magnetosphere [32, 33]. The plasma acts as a conductor and will screen the NS's electric fields until force-free conditions are established, that is, until $\mathbf{E} \cdot \mathbf{B} = 0$.

Once the BH enters the light cylinder of the NS and the battery is established, the electric field configuration changes and the magnetosphere adjusts with those changes. At the large separations of the light cylinder, the plasma is tenuous but in the final stages when the voltage is most powerful, both compact objects should be submerged in the conducting plasma. Consequently, we anticipate that some of the emf generated by the orbital motion is screened and forces are muted. However, as with the pulsar, there must be gaps in which screening is inefficient and across which particles must be accelerated. Additionally, current sheets could act to dissipate the BH-battery power.

We currently do not know the degree to which the voltage is reduced by screening. In the future, global particle-in-cell codes could assess the gap structure in a BHNS magnetosphere. To make simple estimates, we continue to use the full power of the battery in the calculation of the curvature radiation, aware that screening could significantly reduce the estimates.

To obtain the primary curvature radiation spectrum, we assume a distribution in energy of the magnetosphere electrons and positrons. The spectrum of curvature radiation is given by integrating the one-electron spectrum multiplied by the num-

ber distribution of charged particles.

$$P_C(\nu, t) = \int_{\gamma_{\min}}^{\gamma_{\max}} N(\gamma) \frac{dP_C}{d\nu} d\gamma \quad (9)$$

where $dP_C/d\nu$ represents the curvature radiation power per unit frequency [e.g, 34]. We model the population as a power law in the relativistic Lorentz factor γ ,

$$N(\gamma)d\gamma = N_0\gamma^{-p}d\gamma. \quad (10)$$

The normalization constant N_0 is chosen so that the total bolometric luminosity matches Eq. (5)

$$N_0 = \frac{\mathcal{P}}{\int \int \gamma^{-p} \frac{dP_C}{d\nu} d\gamma d\nu}, \quad (11)$$

so that the magnetosphere number density ($\sim N_0/r^3$) is set by the physics of curvature radiation and the requirement that the magnetosphere maximally radiates the BH-battery power.

The spectrum then depends on the energy distribution of electrons and positrons through the exponent p , and the time-dependent minimum and maximum Lorentz factors of particles in the magnetosphere $\gamma_{\max}(t)$ and $\gamma_{\min}(t)$ that we must input from the physical model of the BHNS battery. As the spectrum is not greatly dependent on the minimum γ or the power law index p (see the Appendix), we leave these as free parameters. The shape of the spectrum will depend on the choice of $N(\gamma)$, but, for what follows, the most important consideration will be where the high energy end of the spectrum is cut off. This is set by the maximum electron Lorentz factor in the magnetosphere.

We approximate the maximum γ as the largest radiation-reaction limited Lorentz factor in the magnetosphere. Electrons and positrons are accelerated along magnetic-field lines to radiation-reaction limited velocities given by solving,

$$ec|\mathbf{E}_{\parallel}|(1 - \gamma^{-2})^{1/2}_{\max} = \frac{2ce^2\gamma_{\max}^4}{3\rho_c^2} \quad (12)$$

for the Lorentz factor γ_{\max} . Here ρ_c is the radius of curvature of magnetic-field lines. We evaluate ρ_c for a dipole magnetic field in the binary equatorial plane, $\rho_c = R_{\text{NS}}/3\sqrt{r/R_{\text{NS}}}$. We use the horizon electric field sourced by the potential drop Eq. (4) to estimate a maximum value of the accelerating electric fields, $|\mathbf{E}_{\parallel}| \approx |\mathbf{E}| \sim \frac{V_{\text{BH}}}{R_{\text{H}}}$ where R_{H} is the radius of the BH horizon.

Then the radiation-reaction limited Lorentz factor of electrons/positrons, at the BH horizon is

$$\gamma_{\max} \approx 4.2 \times 10^7 \left(\frac{r}{6GM/c^2} \right)^{-5/8} \left(\frac{B_{\text{NS}}}{10^{12} \text{ G}} \right)^{1/4}, \quad (13)$$

choosing fiducial parameters $R_{\text{NS}} = 10^6 \text{ cm}$ and $M_{\text{BH}} = 10M_{\odot}$. Electrons and positrons will emit curvature radiation with characteristic energy

$$\epsilon_{\gamma} = \frac{3hc}{4\pi\rho_c} \gamma^3 \approx 1.8 \text{ TeV} \left(\frac{\gamma}{4.2 \times 10^7} \right)^3. \quad (14)$$

⁶ When the energy of curvature photons is great enough, they will interact with the magnetosphere magnetic and electric fields and produce electron-positron pairs. As the curvature photons are not locked to move along magnetic-field lines, the secondary pairs can have a non-negligible component of motion transverse to the magnetic field, resulting in a secondary synchrotron spectrum.

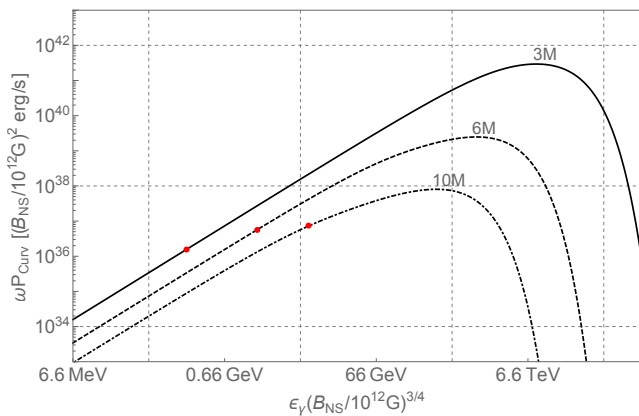


FIG. 3: The spectra of primary curvature radiation at times corresponding to binary separations $10GM/c^2$, $6GM/c^2$, and $3GM/c^2$ (dot-dashed, dashed, solid) scaled to $B_{\text{NS}} = 10^{12}G$ (factors of G and c are omitted in the labels). We use an electron-energy power law index of $p = 2.0$ and a minimum Lorentz factor set by radiation reaction in the outer magnetosphere. Dependence on both parameters is minimal (see the Appendix). The red dots indicate photon energies above which the magnetosphere is opaque to pair production via $\gamma + B$ interactions.

We plot a representative curvature radiation spectrum for a fiducial $10M_{\odot}$ BH with maximal spin. The dependence of the curvature spectrum on γ_{min} and p is explored in the Appendix.

In agreement with previous works [1, 2], Figure 3 shows that the BHNS curvature radiation can be very high energy, $> \text{TeV}$, near merger. In the following section, we point out that this curvature radiation will be prone to copious pair production through interaction with the strong electromagnetic fields of the magnetosphere as well as photon-photon collisions. The pair production will further populate the electron-positron plasma surrounding the binary. Depending on the efficiency at which pairs are produced from the available energy of the BH battery, the magnetosphere will become optically thick to curvature photons. This trapped radiation can power a fireball, which we now characterize.

III. FIREBALL

As the BH and NS draw closer, the energy available to accelerate particles increases as $r^{-3}v$, resulting in a higher density of higher energy curvature photons. A consequence is pair production through the interaction of the magnetic field and high-energy photons ($\gamma + B \rightarrow e^+ + e^-$) and through photon collisions ($\gamma + \gamma \rightarrow e^+ + e^-$), preventing the highest energy curvature photons from escaping the magnetosphere. The result is an optically thick pair+radiation fluid, which will expand outwards under its own pressure until pair production becomes disfavored and radiation can escape; the result is a fireball.

A. Pair production

The optical depth to $\gamma + B \rightarrow e^+ + e^-$, at binary separation r is

$$\tau_{\gamma B} = r \left[\frac{4.4}{e^2/(\hbar c)} \frac{\hbar}{m_e c} \frac{B_q}{B_{\perp}} \exp\left(\frac{4}{3\xi}\right) \right]^{-1} \quad (15)$$

$$\xi \equiv \frac{\hbar\omega}{2m_e c^2} \frac{B_{\perp}}{B_q}$$

$$B_q \equiv \frac{m_e^2 c^3}{e\hbar} \approx 4.4 \times 10^{13} G$$

$$B_{\perp} \equiv \text{Min} \left\{ x/(R_{\text{NS}}/3\sqrt{r/R_{\text{NS}}}), 1 \right\} B(r)$$

for photons with $\hbar\omega \gtrsim 2m_e c^2$. The quantity in brackets is the mean free path for pair production given by Refs. [33, 35], B_q is a natural quantum mechanical measure of magnetic-field strength, and B_{\perp} is the component of magnetic field perpendicular to the photon trajectory. The quantity in curly brackets in the last line of Eq. (15) is the sine of the angle between a photon trajectory and the magnetic-field direction, which is simply the distance x a photon has traveled in direction initially tangent to a field line, divided by the radius of curvature of field lines. As a characteristic value, we take the radius of curvature to be that of a dipole field line which goes through the center of the BH at binary separation r . This approximation assumes that $\xi \ll 1$, which is always true initially when $x = 0$ and $B_{\perp} = 0$. In practice we cap $\xi \leq 1$ because we are only interested in when $\tau_{\gamma B} \rightarrow 1$. After this point the $\gamma + \gamma \rightarrow e^+ + e^-$ process will also become important, so we need not rely solely on the above calculation (see below).

For very high-energy photons, the optical depth limits to very large values but drops exponentially for lower energy photons, generated earlier in the binary inspiral. To capture the steep dependence of the $\gamma + B \rightarrow e^+ + e^-$ optical depth on photon frequency, we evaluate $\tau_{\gamma B}$ at a frequency near the peak of the time-dependent curvature radiation spectrum (see Figure 3).

The red dots plotted on top of the spectra of Figure 3 show the frequency at which the $\gamma + B \rightarrow e^+ + e^-$ optical depth (Figure 4) becomes unity for three different snapshots during the inspiral. Above the frequency indicated by the red dots in Figure 3, photons pair produce with the magnetic field before escaping the magnetosphere.

The optical depth for $\gamma + \gamma \rightarrow e^+ + e^-$ at binary separation r is

$$\tau_{\gamma\gamma} \approx r n_{\gamma*} \sigma_{\gamma\gamma} \quad (16)$$

where we use a collision cross section $\sigma_{\gamma\gamma} = 11/180\sigma_T$ [36, 37] averaged over photon energy and written in terms of the Thomson scattering cross section σ_T .

Once the magnetosphere becomes optically thick to $\gamma + B$ pair production, we assume that the radiation plus pair plasma thermalizes. Then we may approximate $n_{\gamma*}$ as the portion of the Planck spectrum with sufficient energy to produce pairs

$$n_{\gamma*} = \frac{8\pi}{c^3} \int_{2m_e c^2/h}^{\infty} \frac{\nu^2 d\nu}{e^{h\nu/kT} - 1}. \quad (17)$$

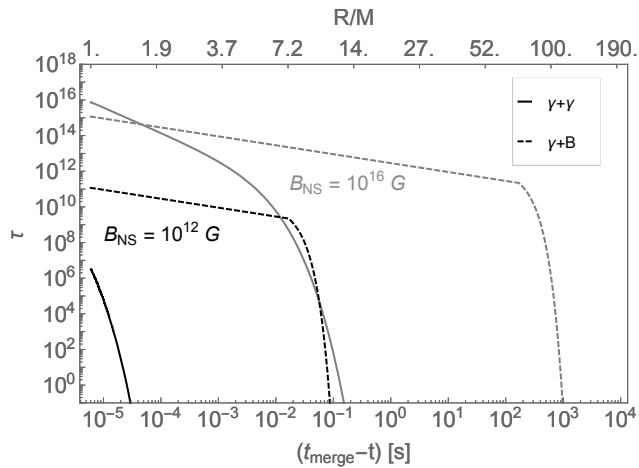


FIG. 4: The optical depth to the different pair producing processes. The magnetosphere curvature photons are trapped by $\gamma + B$ early on, $\gamma + \gamma$ also becomes relevant for magnetosphere photons just before merger. The $\gamma + B$ optical depth is computed at a time-dependent frequency near the peak of the primary curvature spectrum. Factors of G and c are omitted in the upper x-axis label.

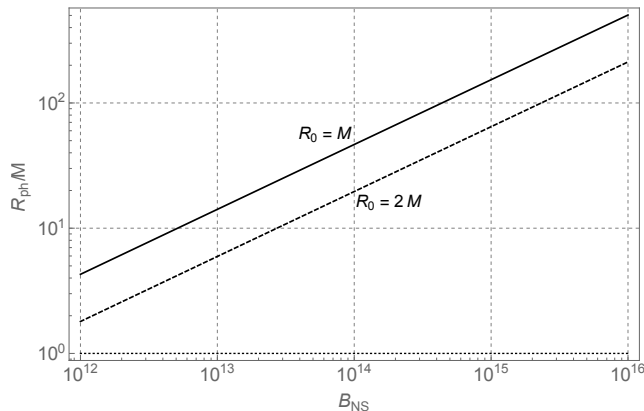


FIG. 5: The radius of the photosphere as a function of NS magnetic-field strength, for different assumed radii of energy injection $R_0 = GM/c^2, 2GM/c^2$. Factors of G and c are omitted in the figure labels.

which is an underestimate as any two photons with energies $\sqrt{\epsilon_1 \epsilon_2} \geq 2m_e c^2$ are favored to create pairs upon collision, not just those above $2m_e c^2$.

Figure 4 shows the optical depth of the magnetosphere to both $\gamma + B$ and $\gamma + \gamma$ pair production as a function of time during inspiral for NS magnetic-field strengths which bracket the expected range. The $\gamma + B$ process becomes important first, when curvature-photon energies surpass a critical value (see the red dots plotted on the spectra of Figure 3). Much closer to merger, $\gamma + \gamma \rightarrow e^- + e^+$ also becomes an important source of pair production and hence photon opacity.

The high optical depths in Figure 4 suggest copious pair production due to $\gamma + B$ earlier in the inspiral. If this process thermalizes the radiation and pairs, then our assumption of a Planck gas in the computation of the subsequent $\gamma + \gamma$ optical

depth is warranted. The important point is that, with the large magnetic-field strengths and energy densities present in the BHNS magnetosphere near merger, both pair production processes will be favored. Hence we reason that pair production traps and thermalizes the power generated by the BH battery.

We can conclude from this section that the era of curvature radiation gives way to a hot fireball in the final moments before merger. Curvature radiation becomes trapped when $\tau_{\gamma B} = 1$ (Figure 4), from which we find that high-energy curvature radiation will no longer escape for the final 0.1s ($B/10^{12}G$) of inspiral. Figure 2 shows that at 0.1s ($B/10^{12}G$) before merger the BH-battery luminosity, and thus the maximum power in curvature radiation, is $\sim 10^{38} \text{erg s}^{-1} (B/10^{12}G)^{1/2}$, a factor of $\sim 10^7 (B/10^{12}G)^{3/2}$ lower than the BH-battery peak power at merger. Consequently, at $P_C \lesssim 10^{38} \text{erg s}^{-1} (B/10^{12}G)^{1/2}$, the ramp up in high-energy curvature radiation will likely only be observable within the galaxy.

The subsequent fireball however, could be observable at cosmological distances. We characterize the emission from the fireball in the following section.

B. Expansion and emission

The optically thick pair plus radiation fluid – the fireball – will expand under its own pressure. The alternative is that the fireball falls right down into the BH, although we argue this will not happen. To determine if the fireball will expand, we consider the imbalance of gravity and the mechanical pressure P of the fluid. The condition for expansion is

$$\frac{dP}{dr} \sim \frac{P}{R_0} > \rho \frac{GM}{R_0^2}, \quad (18)$$

where R_0 is the initial scale over which energy is injected by the battery. For a radiation dominated fluid $P = \rho c^2/3$ and then

$$R_0 \gtrsim \frac{GM}{c^2}, \quad (19)$$

dropping all numerical factors. Radiation pressure alone can cause the fireball to expand. We note that the force balance is marginal at small size scales and will depend on the density distribution in addition to magnetic pressure, both of which will likely increase the outward pressure of the fireball and should be treated in a more detailed calculation. Considering the high temperature at merger, the pressure may be dominated by pairs, not radiation. In this limit, $kT > m_e c^2$, the total pair pressure is 7/4 the radiation pressure and the fireball will still expand.

After merger, the magnetic fields responsible for $\gamma + B$ pair production will decay without the NS to anchor them (see however §IV). This means that, after merger, only $\gamma + \gamma$ pair production and electron scattering will trap photons in the expanding fireball. To track the expansion of the fluid from this point, we estimate its properties during and after merger.

Because the optically thick, pair plus radiation fluid is assumed to be in thermal equilibrium, we can estimate the temperature of the fluid as

$$T(r) = \left(\frac{\mathcal{P}(r)}{4\pi r^2 \sigma} \right)^{1/4}, \quad (20)$$

as a function of the binary separation throughout inspiral, where $\mathcal{P}(r)$ is the power emitted by the BH battery at separation r , and σ is the Stefan-Boltzmann constant. Then the initial temperature of the fireball T_0 is the final temperature before the magnetic fields are swallowed/dissipated and the pair plus radiation fluid is released to expand. Evaluating this temperature at a final binary separation of $R_0 \sim GM/c^2$ gives an initial injection temperature of

$$kT_0 = 85 \text{ keV} \left(\frac{B_{\text{NS}}}{10^{12} \text{ G}} \right)^{1/2}. \quad (21)$$

We treat the fireball as an adiabatically expanding, relativistic fluid. As the fluid expands to a radial size scale R , it cools as $T = T_0(R/R_0)^{-1}$. At a large enough R , $\gamma + \gamma$ pair production and electron scattering will no longer trap photons, and radiation escapes.

The $\gamma + \gamma$ optical depth is given by Eq. (16) and the optical depth to electron/positron scattering is,

$$\tau_{\text{es}} \sim r n_{\pm} \sigma_{\text{T}}, \quad (22)$$

where σ_{T} is the Thomson scattering cross section, and n_{\pm} is the rest-frame, pair number density in thermal equilibrium. We estimate n_{\pm} as the electron number density [e.g., 38], true for $kT \ll m_e c^2$, which is always the case in the photosphere for $B_{\text{NS}} \lesssim 10^{16} \text{ G}$. Then,

$$n_{\pm} \approx \frac{4\pi^{3/2}}{h^3} (2m_e kT)^{3/2} \exp\left(-\frac{m_e c^2}{kT}\right) \quad (23)$$

Eventually the fireball expands until the temperature has dropped sufficiently for both $\tau_{\gamma\gamma} \leq 1$ and $\tau_{\text{es}} \leq 1$. We call this radius the photosphere radius R_{ph} . We find that the fireball first becomes transparent to $\gamma + \gamma$ pair production and then to electron scattering at a larger, but similar radius (within a factor of a few). Hence the photosphere is defined where $\tau_{\text{es}}(R_{\text{ph}}) \equiv 1$. The photosphere radius as a function of NS magnetic-field strength is plotted in Figure 5 for two choices of the initial size of the fireball, GM/c^2 and $2GM/c^2$ (we assume a fiducial $R_0 = GM/c^2$ throughout).

We estimate the Lorentz factor of the adiabatically expanding fluid as $\gamma = R/R_0$ [38] for $R \gg R_0$. Then emission from the photosphere will be that of a blackbody boosted at Lorentz factor $\gamma_{\text{ph}} = R_{\text{ph}}/R_0$. Such a boosted blackbody looks like the rest-frame blackbody but with an effective temperature

$$T_{\text{eff}} = \frac{T_{\text{ph}}}{\gamma_{\text{ph}}(1 - v_{\parallel}/c)} \equiv DT_{\text{ph}} \quad (24)$$

where D is the doppler factor, T_{ph} is the temperature in the rest frame of the photosphere, and $v_{\parallel} = v \cos \theta$ is the line-of-sight velocity, where θ is the angle from observer line of

sight. Because the shell is expanding spherically, each patch of the expanding photosphere will have a different effective temperature and the observed, time-dependent spectrum will be a sum of the spectra of all patches on equivalent light travel time surfaces [e.g., 39]. We do not include such details here; in §V we integrate the line-of-sight dependent blackbody spectra over the photosphere to find a composite spectrum, but for now we make a simple estimate for the peak energy of blackbody emission.

The total photospheric emission will not deviate greatly from blackbody, and the majority of emission will come from the portion of the expanding sphere for which the Doppler factor is positive, where the angle to the line of sight is less than $1/\gamma$. For highly relativistic expansion, the blue-shifted temperature Eq. (24) becomes $T = \gamma T_{\text{ph}}$ at $\theta = 1/\gamma$ and $T = 2\gamma T_{\text{ph}}$ at $\theta = 0$. For simplicity we use that the photosphere emission is a blackbody with temperature $T \sim \gamma T_{\text{ph}}$. Then because the photosphere temperature is related to the initial temperature as $T_{\text{ph}} = T_0(R_0/R) = T_0/\gamma_{\text{ph}}$, the observed blackbody temperature is simply $T = T_0$ [see also 38]; the observed temperature is the same as the initial injection temperature of Eq. (21) (the effects of gravitational redshift are negligible for $R_{\text{ph}} \gg R_0$). For a fiducial energy-injection size scale of $R_0 = GM/c^2$, the *observed* photosphere emission will peak at

$$h\nu_{\text{peak}} = 0.24 \text{ MeV} \left(\frac{B_{\text{NS}}}{10^{12} \text{ G}} \right)^{1/2}, \quad (25)$$

ranging from hard x rays to γ rays.

From the pair density at the photosphere we estimate the plasma frequency to be,

$$\nu_{\text{pl}} = \sqrt{\frac{n_{\pm} e^2}{\pi m_e}} \lesssim 4.4 \times 10^{12} \text{ Hz} \left(\frac{B_{\text{NS}}}{10^{12} \text{ G}} \right)^{-0.26}. \quad (26)$$

The blackbody emission is not shorted out by the pair plasma, however, emission in the far-infrared and at longer wavelengths does not escape the photosphere.

Because the photosphere is generated due to a decrease in pair density, there will be no detectable signal from blue-shifted pair annihilation [see also 38, 40]. The ratio of energy in pairs to that in radiation at the photosphere is small,

$$\frac{E_{\pm}}{E_{\gamma}} \simeq \frac{m_e c^2 n_{\pm} c}{\sigma T_{\text{ph}}^4} < 10^{-8}. \quad (27)$$

Finally we note that, because the fireball must expand out to its photosphere size before it can radiate, the EM transient predicted here will occur at least $R_{\text{ph}}/c \sim 0.2 \text{ msec} \sqrt{B/10^{12} \text{ G}}$ after the initial energy injection. If energy injection is associated with merger, then this EM signature will occur shortly after peak gravitational-wave emission. Hence gravitational waves from the inspiral stage, which will trigger a LIGO detection, will also warn of this EM counterpart.

To summarize, we predict that, as the binary nears the final few GM/c^2 in binary separation, high-energy curvature radiation will produce pairs by interacting with other photons

and also the magnetic field. The BHNS magnetosphere becomes optically thick to pair production, trapping the energy injected by the BH battery. This energy injection causes the optically thick pair plus radiation fluid to expand outwards until the temperature drops below that which favors a high pair density. At this point pair production and electron scattering no longer contain the photons and they escape. For initial NS field strengths of $10^{12} \rightarrow 10^{16} \text{G}$, the observable radiation is characterized as:

- Blackbody radiation with a peak photon energy $h\nu \sim 0.24 \text{ MeV} \sqrt{B_{\text{NS}}/10^{12} \text{G}}$.
- A bolometric luminosity of up to $10^{45} \text{ erg s}^{-1} (B_{\text{NS}}/10^{12} \text{G})^2$.
- Defining $\Delta t_{42}(B_{\text{NS}})$ as the time before merger over which the BH is supplying power above $10^{42} \text{ erg s}^{-1}$, and associating this with the emission timescale, the burst times to the closest order of magnitude are $\Delta t_{42}(10^{12} \text{G}) \sim 10^{-3} \text{ s}$, $\Delta t_{42}(10^{14} \text{G}) \sim 0.1 \text{ s}$, $\Delta t_{42}(10^{16} \text{G}) \sim 10 \text{ s}$.

We next consider a post-merger signal and the observability of both merger and post-merger events.

IV. POST MERGER

When the BH swallows the NS, a magnetic flux is deposited onto the BH, magnetizing the hole. The no-hair theorem suggests the BH, in vacuum, must shed the absorbed B field on order the BH light crossing time, in very long-wavelength, $\sim R_H$, radiation [e.g., 41]. However, [42] have argued, in the context of NS collapse to a BH, that because the BH is immersed in magnetosphere plasma, the no-hair theorem is not applicable and the BH may retain a magnetic field anchored in a remnant magnetosphere for longer. The situation is similar to our case where the BH swallows the NS. In the limit of a nonresistive plasma, magnetic-field lines are frozen into the plasma of the magnetosphere. Because of the frozen-in condition, field lines which connect the NS surface to infinity before merger must also connect the BH horizon to infinity after merger, while closed field lines are swallowed along with the NS. Hence a magnetic field is anchored onto the BH merger remnant. For a resistive plasma, the field will decay on the resistive timescale of the magnetosphere. As a consequence, the remnant BH could generate an electromagnetic signature through the BZ mechanism [22, 42].

The initial BZ power can be written in terms of the magnetic flux deposited onto the BH horizon as

$$P_{\text{BZ}} \sim \frac{\phi^2}{4\pi c} \left(\frac{Sc}{R_H(S)} \right)^2 \quad (28)$$

$$\sim 3 \times 10^{42} \text{ erg s}^{-1} S^2 \left(\frac{B_{\text{NS}}}{10^{12} \text{G}} \right)^2 \left(\frac{2\pi/\Omega_{\text{orb}}}{1 \text{msec}} \right)^{-2} \left(\frac{R_H(S)}{\text{GM}/c^2} \right)^{-2}$$

where S is the dimensionless BH spin related to the BH angular momentum by $J = SGM^2/c$, $R_H(S)$ is the spin dependent horizon radius, and $2\pi/\Omega_{\text{orb}}$ is the binary orbital period.

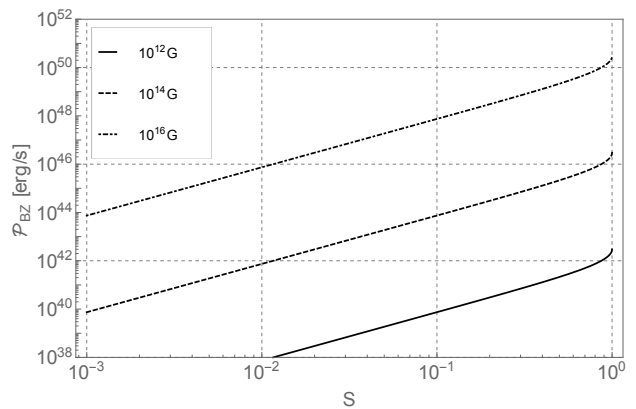


FIG. 6: The power available to the post-merger, spinning BH remnant as a function of remnant spin and NS magnetic-field strength. This power is generated from the Blandford-Znajek process and the flux of open NS magnetic-field lines, Eq. (28). This maximal power will decay as the remnant magnetosphere decays on the resistive timescale.

In the second line we have approximated the magnetic flux thrown onto the BH as the flux of open magnetic-field lines at the NS polar caps [32, 42],

$$\phi = 2\pi B_{\text{NS}} R_{\text{NS}}^2 \sin^{-1} \left(\frac{R_{\text{NS}} \Omega}{c} \right), \quad (29)$$

where, in the single NS case, Ω is the NS spin angular frequency, but here the light cylinder, and hence the footprint of open field lines on the NS surface, is determined by the orbital velocity in addition to the NS spin. Approximating Ω as the orbital angular frequency near merger, Figure 6 plots the initial power available to the post-merger BH as a function of BH spin.

Notice that the post-merger BZ power scales as M^{-2} through $R_H(S)$ whereas the usual BZ power scales as M^2 . The BZ power depends on the square of the magnetic flux deposited onto the BH, which in the standard case, scales with the squared BH surface area M^4 ; adding also the dependence on horizon angular velocity, which scales as M^{-2} , gives the usual M^2 scaling. In the BHNS merger case however, the magnetic flux is set not by the BH size, but by the available flux brought in by the NS, so indeed larger BHs emit less BZ power.

Such a post-merger event will likely generate a relativistically beamed jet which peaks at maximum luminosity given by Figure 6 and then decays with the decaying BH magnetosphere. If the BH can hold onto the magnetosphere for a long enough time, such an event might generate a type of afterglow to the BHNS merger. Assuming that the post-merger signal $^{-2}$ begins at the same time as fireball expansion, at merger, then the peak luminosity of the post merger signal would be observed $R_{\text{ph}}/c \sim 0.2 \text{ msec} \sqrt{B/10^{12} \text{G}}$ before the blackbody fireball emission. We mention this as it is of observational interest and an avenue to pursue in developing the full portrait of the BH battery.

V. OBSERVABILITY

The Fermi GBM [GBM 43] is well suited for detecting the transients described above. It has an energy range of 0.008 \rightarrow 30 MeV, capturing the peak of emission predicted for binaries with 10^{12} to $\sim 10^{16}$ G NS magnetic-field strengths (Eq. 25). It has a $2\mu\text{s}$ timing resolution, sufficient to resolve the $\gtrsim 1\text{msec}$ bursts. The Fermi GBM also operates with a nearly full-sky field of view (currently operating at 9.5 sr with a 10 sr goal), important for catching such possibly rare transients.

We estimate the photon flux at the instrument by assuming emission from a blackbody with Doppler boosted (Eq. 24) and cosmologically redshifted temperature. The photon flux at the GBM is

$$F_{\text{obs}} = 2\pi \int_0^{\theta_c} \int_{\nu_{\text{min}}}^{\nu_{\text{max}}} \frac{2\nu^2}{c^2} \frac{\cos\theta \sin\theta d\nu d\theta}{\exp\left[\frac{h\nu(1+z)}{kT_{\text{eff}}(\theta)}\right] - 1} \quad (30)$$

$$\theta_c = \frac{R_{\text{ph}}}{d_A(z)}$$

$$d_A(z) = \frac{c}{H_0} \int_0^z \frac{dz'}{\sqrt{\Omega_M(1+z')^3 + \Omega_\Lambda}}$$

$$T_{\text{eff}}(\theta) = T_{\text{ph}} \left[\gamma \left(1 - \frac{v}{c} \cos\left(\frac{\pi}{2} \frac{\theta}{\theta_c}\right) \right) \right]^{-1}$$

where d_A is the angular diameter distance in the 2015 Planck cosmology with $\Omega_M = 0.308$, $\Omega_\Lambda = 1 - \Omega_m$, and $H_0 = 67.8 \text{ km s}^{-1} \text{ Mpc}^{-1}$ [44], and where integration is over the solid angle of the photosphere at redshift z , and over the frequency limits of the GBM. We use the minimum detectable flux for the GBM to solve $F_{\text{obs}}(z) = F_{\text{min}}$ for the maximum observable redshift to which BHNS transients could be observed. Using the GBM on-board trigger sensitivity, $F_{\text{min}} = 0.71 \text{ cm}^{-2} \text{ s}^{-1}$ [43], we find

$$\begin{aligned} d_M^{\text{max}}(B_{\text{NS}} = 10^{12}\text{G}) &\sim 9 \text{ Mpc}; & z^{\text{max}} &= 0.002 \\ d_M^{\text{max}}(B_{\text{NS}} = 10^{13}\text{G}) &\sim 49 \text{ Mpc}; & z^{\text{max}} &= 0.011 \\ d_M^{\text{max}}(B_{\text{NS}} = 10^{14}\text{G}) &\sim 270 \text{ Mpc}; & z^{\text{max}} &= 0.064 \\ d_M^{\text{max}}(B_{\text{NS}} = 10^{15}\text{G}) &\sim 1.3 \text{ Gpc}; & z^{\text{max}} &= 0.339 \\ d_M^{\text{max}}(B_{\text{NS}} = 10^{16}\text{G}) &\sim 5.1 \text{ Gpc}; & z^{\text{max}} &= 1.886, \end{aligned} \quad (31)$$

which we have quoted in terms of the comoving radial distance d_M and the corresponding redshift. The $\gtrsim 10^{13}\text{G}$ binaries are detectable out to beyond the initial LIGO volume, while only the $\gtrsim 10^{14.5}\text{G}$ binaries are detectable out to approximately the advanced LIGO volume for BHNS mergers [redshift $z \sim 0.1$; 45].

To estimate the number of expected detections out to z^{max} we need to know the rate of BHNS mergers as a function of B_{NS} , and we need to know what fraction of those mergers generate the signal derived here. BHNS coalescence rates are computed by Ref. [45]. They predict between 6×10^{-4} and 1 BHNS coalescences per Mpc^3 per Myr with a most probable rate of 0.03 per Mpc^3 per Myr. Estimating the number of nondisrupting BHNS mergers with a given NS magnetic-field strength is beyond the scope of the present work. Instead, we

B_{NS} [G]	Minimum	Expected	Maximum
10^{12}	1.4×10^{-6}	6.9×10^{-5}	2.3×10^{-3}
10^{13}	2.4×10^{-4}	1.2×10^{-2}	0.4
10^{14}	3.9×10^{-2}	2.0	66
10^{15}	5.0	248	8.3×10^3
10^{16}	267	1.3×10^4	4.5×10^5

TABLE I: Expected number of Fermi GBM events in units of $[\text{yr}^{-1}] f_{\text{fb}}(B_{\text{NS}})$ where $f_{\text{fb}}(B_{\text{NS}})$ is the fraction of BHNS coalescences with NS magnetic-field strength B_{NS} and which will not tidally disrupt the NS and will generate the signal predicted here. B_{NS} is the NS surface magnetic-field strength.

parametrize the fraction of BHNS mergers which generate the signal predicted here as $f_{\text{fb}}(B_{\text{NS}})$. Using the calculated maximum detection redshifts we calculate the comoving detection volume. Using this maximum detection volume, coalescence rates with $f_{\text{fb}} = 1$, and a 10 sr field of view, Table I lists the expected number of events that FERMI GBM could detect per year.

For BHNS binaries with $B_{\text{NS}} \lesssim 10^{14}\text{G}$, these optimistic, expected rates of detection drop below 1 per year. To probe the binaries with $B_{\text{NS}} \gtrsim 10^{13}\text{G}$ at a rate of $\sim 1.0 f_{\text{fb}} \text{ yr}^{-1}$, future x-ray instruments must have full-sky sensitivities of $\sim 10\times$ the FERMI GBM. They must have sensitivities $\sim 600\times$ the GBM to reach $B_{\text{NS}} \gtrsim 10^{12}\text{G}$ binaries at the same rate.

Assuming our model roughly captures the BHNS luminosity and spectrum, there are two options for BHNS mergers with $B_{\text{NS}} \gtrsim 10^{14}\text{G}$. Either we have already observed the high-magnetic-field BHNS fireballs as a subclass of short gamma-ray bursts (sGRBs), or we have not, and the fraction of nondisrupting BHNS binaries with such magnetic fields f_{fb} is very small.

The BHNS fireball could compose a subclass of the sGRB population if a, yet unknown, mechanism saturates NS field strengths to maximal $\geq 10^{15}\text{G}$ values near merger, then the rates predicted here become comparable to the inferred (beaming angle dependent) rates of sGRBs, $8 \rightarrow 1100 \text{ Gpc}^{-3} \text{ yr}^{-1}$ from Swift measurements [46]. The analysis of §III allows emission from $\sim 10^{15}\text{G}$ fireballs to be of order seconds, consistent with sGRB time scales.

Alternatively, evidence has been found that a class of sGRBs, making up 10 to 25 percent of the total, may be at a near $z \leq 0.025$ [47]. These would be a different class than those sGRBs for which distances can be measured out to a Gpc through afterglows [*e.g.*, 48]. The implication is that a class of sGRBs has a much lower luminosity engine, which could be powered by the $B_{\text{NS}} \sim 10^{13}\text{G}$ BHNS transients discussed here. This possibility, however, requires an explanation for increased rates of BHNS mergers in the local universe.

If the BHNS fireball is not a subset of the observed GRB population, then, based on the present nondetection, we may place limits on the fraction of binaries which carry $B_{\text{NS}} \gtrsim 10^{14}\text{G}$, to merger. Using the expected rates and the total operation time of the GBM at its current sensitivity (~ 5 years) we find that $f_{\text{fb}}(\geq 10^{15}\text{G}) \lesssim 10^{-3}$ and $f_{\text{fb}}(\geq 10^{16}\text{G}) \lesssim 10^{-4}$.

Where the inequalities assume that f_{fb} is a steeply decreasing function of magnetic-field strength for $B_{\text{NS}} > 10^{14}\text{G}$.

Another possibility is that these upper limits for the luminosity of the signal are indeed overestimates and mechanisms such as screening in the magnetosphere greatly damp power output; continued electromagnetic, as well as future gravitational wave, observations will test this. Concurrently, further modeling of the BHNS magnetosphere would hone the expected signal and the derived rates of detection.

The above analysis relies on a choice of $R_0 = GM/c^2$ for the size scale of energy injection. This is a natural choice, however we discuss briefly the dependence of our results on injection radius. If we go with a large value of $R_0 = 2GM/c^2$, then less energy is injected over a larger volume and the initial temperature of the fireball drops to 18 keV $(B_{\text{NS}}/10^{12}\text{G})^{1/2}$ from our fiducial 85 keV $(B_{\text{NS}}/10^{12}\text{G})^{1/2}$ for $R_0 = GM/c^2$. This corresponds to a peak black body temperature of 52 keV $(B_{\text{NS}}/10^{12}\text{G})^{1/2}$, down from the fiducial 0.24 MeV $(B_{\text{NS}}/10^{12}\text{G})^{1/2}$. These lower energies are still within the energy range of the Fermi GBM, but a combination of less injected energy, smaller photosphere sizes (Figure 5) (and hence smaller expansion speed at the photosphere) decrease the maximum observable distance of the fireball by a factor of ~ 3 and also decreases the expected rates (Table I) by one to two orders of magnitude.

VI. CONCLUSION

We have used BH-battery energetics to argue that near merger, a BHNS will produce an electromagnetic transient. A spectrum of high-energy ($\sim \text{TeV}$) curvature radiation will escape the magnetosphere before the last 0.1s $(B/10^{12}\text{G})$ of inspiral. This signature will only reach luminosities of $\sim 10^{38}\text{erg s}^{-1} (B/10^{12}\text{G})^{1/2}$ before being quenched by pair production and fueling the more luminous fireball transient. The expanding fireball will become transparent and emit as a blackbody in the x-ray to γ -ray range for of order $10^{-3} \rightarrow 10$ seconds depending on the NS magnetic-field strength. The observed luminosity can peak at $10^{45}\text{ erg s}^{-1}$ for a 10^{12}G NS magnetic field or up to $10^{53}\text{ erg s}^{-1}$ for magnetar strength fields. If the BH can hold onto the NS magnetic fields after merger through a slow decay of the magnetosphere [42], a spinning remnant BH could power a relativistic jet with bolometric luminosity up to 2 orders of magnitude lower than the fireball luminosity, peaking at $\sim 0.2\text{ msec}\sqrt{B/10^{12}\text{G}}$ before the observed fireball emission, and decaying on the unknown resistive timescale of the magnetosphere.

The prospects for detecting the bright, fireball transient are dependent on the (unknown) distribution of NS magnetic-field

strengths B_{NS} at merger. To explore these prospects, we have left the NS surface magnetic-field strength as a free parameter. Conversely, BHNS merger rates allow our model to put constraints on B_{NS} at merger. Given predicted BHNS merger rates, the majority of BHNS mergers must have $B_{\text{NS}} > 10^{14}\text{G}$ to be detectable by Fermi GBM at the rate of $\sim 1\text{ yr}^{-1}$. If $B_{\text{NS}} \lesssim 10^{12}$ at merger, as might be expected from the observed pulsar magnetic-field strengths [49], a future x-ray instrument would need a full-sky sensitivity of $\gtrsim 600$ the present FERMI GBM capabilities to detect these EM signatures of BHNS coalescence. If ordered magnetic fields are amplified to $\gtrsim 10^{15}\text{G}$ at merger, then expected FERMI GBM detection rates for the signature in this study climb to rival the gamma-ray burst rate, and may be a subclass of sGRBs [46].

Any observation of a BH-battery transient would be exciting in its own right. With advanced LIGO now operational, the EM counterpart to BHNS coalescence has additional payout potential, offering unique information to extend the astronomical reach of the gravitational-wave observatories.

Acknowledgments

The authors thank Andrei Beloborodov, Brian Metzger, and Sean McWilliams for useful discussions. The authors also thank the anonymous referee for comments that improved the manuscript. D.J.D. acknowledges support from a National Science Foundation Graduate Research Fellowship under Grant No. DGE1144155. J.L. thanks the Tow Foundation for their support. J.L. was also supported by a Guggenheim Fellowship and is a Chancellor's Fellow at Chapman University. This research was undertaken, in part, thanks to funding from the Canada Research Chairs program. NWM was supported in part by the Natural Sciences and Engineering Council of Canada.

Appendix A: Parameter Dependence of Curvature Spectra

Figure 7 plots the curvature radiation spectra, identical to Figure 3, but for different values of the electron-energy power law index p , and the minimum electron Lorentz factor in the magnetosphere, γ_{min} . We vary p from 1.0 to 3.0. We choose minimum Lorentz factors which bracket the range of plausible values: $\gamma_{\text{min}} = 1$, and a minimum radiation-reaction limited Lorentz factor which we compute with Eq. (13) but with electric field at the edge of the binary orbital light cylinder (Ω_{orb}/c) that falls off from its horizon value as r^{-2} [26]. Near merger this is only a few times smaller than the maximum γ computed from the horizon electric fields.

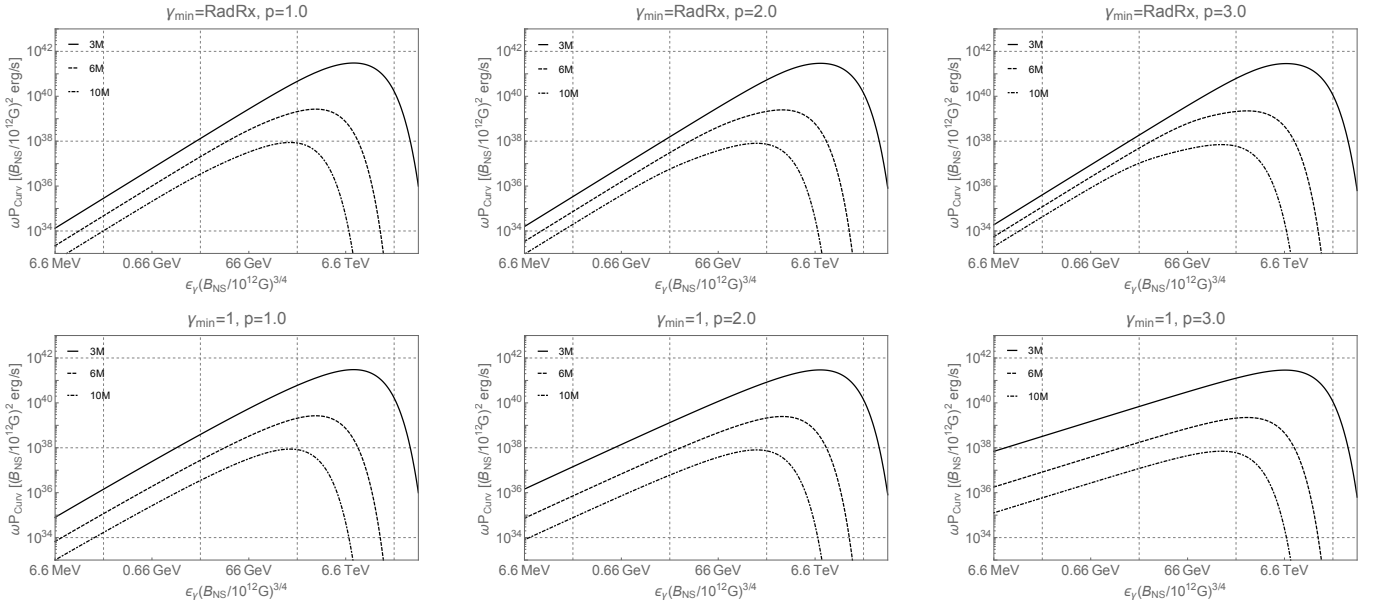


FIG. 7: The spectrum of primary curvature radiation at times corresponding to binary separations of $10M$, $6M$, and $3M$ (dot-dashed, dashed, solid). Each panel is for the labeled minimum electron Lorentz factor and power law index p of electron energies. $\gamma_{\min} = \text{RadRx}$ refers to the radiation reaction limited Lorentz factor at the point of weakest electric field in the region connecting NS and BH (of order a few to 10 times smaller than the maximum Lorentz factor near merger).

-
- [1] S. T. McWilliams and J. Levin, *ApJ* **742**, 90 (2011), 1101.1969.
[2] D. J. D’Orazio and J. Levin, *PRD* **88**, 064059 (2013), 1302.3885.
[3] R. Narayan, B. Paczynski, and T. Piran, *ApJL* **395**, L83 (1992), astro-ph/9204001.
[4] F. Özel, D. Psaltis, R. Narayan, and J. E. McClintock, *ApJ* **725**, 1918 (2010), 1006.2834.
[5] D. Tsang, J. S. Read, T. Hinderer, A. L. Piro, and R. Bondarescu, *Physical Review Letters* **108**, 011102 (2012), 1110.0467.
[6] D. Tsang, *ApJ* **777**, 103 (2013), 1307.3554.
[7] G. M. Harry and LIGO Scientific Collaboration, *Classical and Quantum Gravity* **27**, 084006 (2010).
[8] C. M. F. Mingarelli, J. Levin, and T. J. W. Lazio, *ApJL* **814**, L20 (2015), 1511.02870.
[9] P. Goldreich and D. Lynden-Bell, *ApJ* **156**, 59 (1969).
[10] J. Li, L. Ferrario, and D. Wickramasinghe, *ApJL* **503**, L151 (1998).
[11] R. O. Laine, D. N. C. Lin, and M. Tagger, in *European Planetary Science Congress 2012* (2012), pp. EPSC2012–744.
[12] R. O. Laine and D. N. C. Lin, *ApJ* **745**, 2 (2012), 1201.1584.
[13] M. Vietri, *ApJL* **471**, L95 (1996), astro-ph/9609028.
[14] A. L. Piro, *ApJ* **755**, 80 (2012), 1205.6482.
[15] D. Lai, *ApJL* **757**, L3 (2012), 1206.3723.
[16] C. Palenzuela, L. Lehner, M. Ponce, S. L. Liebling, M. Anderson, D. Neilsen, and P. Motl, *ArXiv e-prints* (2013), 1301.7074.
[17] K. Wu, M. Cropper, G. Ramsay, and K. Sekiguchi, *MNRAS* **331**, 221 (2002), astro-ph/0111358.
[18] S. Dall’Osso, G. L. Israel, and L. Stella, *A&A* **447**, 785 (2006), astro-ph/0507474.
[19] S. Dall’Osso, G. L. Israel, and L. Stella, *A&A* **464**, 417 (2007), astro-ph/0603795.
[20] M. Lyutikov, *PRD* **83**, 064001 (2011), 1101.0639.
[21] R. F. Penna, *PRD* **91**, 084044 (2015), 1503.00728.
[22] R. D. Blandford and R. L. Znajek, *MNRAS* **179**, 433 (1977).
[23] C. Palenzuela, C. Bona, L. Lehner, and O. Reula, *Classical and Quantum Gravity* **28**, 134007 (2011), 1102.3663.
[24] K. Kiuchi, Y. Sekiguchi, K. Kyutoku, M. Shibata, K. Taniguchi, and T. Wada, *PRD* **92**, 064034 (2015), 1506.06811.
[25] V. Paschalidis, Z. B. Etienne, and S. L. Shapiro, *PRD* **88**, 021504 (2013), 1304.1805.
[26] K. S. Thorne, R. H. Price, and D. A. MacDonald, *Black holes: The membrane paradigm* (Yale University Press, 1986).
[27] R. F. Penna, *PRD* **92**, 084017 (2015), 1504.00360.
[28] V. M. Kaspi and M. Kramer, *ArXiv e-prints* (2016), 1602.07738.
[29] S. A. Olausen and V. M. Kaspi, *ApJS* **212**, 6 (2014), 1309.4167.
[30] F. Foucart, *PRD* **86**, 124007 (2012), 1207.6304.
[31] P. C. Peters, *Physical Review* **136**, 1224 (1964).
[32] P. Goldreich and W. H. Julian, *ApJ* **157**, 869 (1969).
[33] M. A. Ruderman and P. G. Sutherland, *ApJ* **196**, 51 (1975).
[34] K. S. Cheng and J. L. Zhang, *ApJ* **463**, 271 (1996).
[35] T. Erber, *Reviews of Modern Physics* **38**, 626 (1966).
[36] Y. Lithwick and R. Sari, *ApJ* **555**, 540 (2001), astro-ph/0011508.
[37] R. Svensson, *MNRAS* **227**, 403 (1987).
[38] B. Paczynski, *ApJL* **308**, L43 (1986).
[39] A. Pe’er and F. Ryde, *ApJ* **732**, 49 (2011), 1008.4590.
[40] J. Goodman, *ApJL* **308**, L47 (1986).
[41] T. W. Baumgarte and S. L. Shapiro, *ApJ* **585**, 930 (2003), astro-ph/0211339.
[42] M. Lyutikov and J. C. McKinney, *PRD* **84**, 084019 (2011),

- 1109.0584.
- [43] *Fermi gbm characteristics* (2015), URL <http://gammaray.msfc.nasa.gov/gbm/>.
- [44] Planck Collaboration, P. A. R. Ade, N. Aghanim, M. Arnaud, M. Ashdown, J. Aumont, C. Baccigalupi, A. J. Banday, R. B. Barreiro, J. G. Bartlett, et al., ArXiv e-prints (2015), 1502.01589.
- [45] J. Abadie, B. P. Abbott, R. Abbott, M. Abernathy, T. Accadia, F. Acernese, C. Adams, R. Adhikari, P. Ajith, B. Allen, et al., *Classical and Quantum Gravity* **27**, 173001 (2010), 1003.2480.
- [46] D. M. Coward, E. J. Howell, T. Piran, G. Stratta, M. Branchesi, O. Bromberg, B. Gendre, R. R. Burman, and D. Guetta, *MNRAS* **425**, 2668 (2012), 1202.2179.
- [47] N. R. Tanvir, R. Chapman, A. J. Levan, and R. S. Priddey, *Nature* **438**, 991 (2005), astro-ph/0509167.
- [48] E. Berger, P. A. Price, S. B. Cenko, A. Gal-Yam, A. M. Soderberg, M. Kasliwal, D. C. Leonard, P. B. Cameron, D. A. Frail, S. R. Kulkarni, et al., *Nature* **438**, 988 (2005), astro-ph/0508115.
- [49] D. Bhattacharya and E. P. J. van den Heuvel, *Phys. Rep.* **203**, 1 (1991).